did not show a hybridization signal (Fig. 4B); this was not a result of DNA degradation because the same blot reprobed with the transgene revealed the expected pattern of hybridization (*9*). Therefore, in line B, the 500-bp genomic sequence has been deleted, and subsequent experiments have revealed a deletion of at least 40 kb of the normal locus (*9*). In mice of the A/B genotype, only the indicative band at 6.0 kb of line A was present, confirming the conclusion that A and B are at the same locus.

Mutations in a number of previously identified loci, localized to various chromosomes, produce mice of small stature as their predominant phenotype (*1*). One of these mutants, pygmy (pg) (*10*), was mapped to chromosome 10 and has many of the characteristic features of the mini-mutation (Fig. 3). Because the 500-bp Apa I–Apa I fragment also mapped to chromosome 10 (*11*), the pygmy and mini loci were tested for allelism. Twelve out of 48 progeny from A/+ and pg/+ matings and 6 out of 35 progeny from B/+ and pg/+ matings were found to be of small stature, which is consistent with the insertional and spontaneous mutants being allelic (*12*).

This allelism was demonstrated by Southern blot analysis of DNA isolated from mice of the indicated genotypes (Fig. 5). Pygmy heterozygotes (pg/+) revealed only a single band at 10 kb, which was representative of the normal locus, and no other bands were apparent. However, in pygmy homozygotes (pg/pg), there was no detectable hybridization, and the same blot rehybridized with c-*kit* as a control probe revealed the appropriate bands. Additionally, mice of genotype B/pg also showed no hybridization signal, whereas A/pg mice revealed only the 6.0-kb disrupted band. Thus, there is a deletion of the 500-bp genomic sequence in the spontaneous mutant, which extends to at least 40 kb (*9*); this finding establishes that there is a disruption at the same locus as in the two insertional mutants. This 500-bp Apa I–Apa I fragment is now routinely used in our laboratory to distinguish between wild-type and heterozygous mice of the spontaneous mutant line rather than the more laborious method of test breeding.

This study describes the molecular characterization of two transgenic insertional mutants at the pygmy locus derived from one founder mouse. The simplest explanation for the pattern of integration is that a single integration event took place that ultimately gave rise to line A. After a few cell divisions, a recombination event occurred in one cell; this event resulted in the deletion of a portion of the tandem array and flanking genomic locus so as to give rise to line B. This would explain the reduced number of copies of the foreign DNA (*13*), the absence of the 500-bp genomic sequence, and the apparent mosaicism of the founder for integration B. Since these initial events no further rearrangements have been observed in line A after ten generations.

Although the pygmy spontaneous mutant has existed for 45 years, it has remained somewhat enigmatic. Unlike the well-characterized dwarf syndromes in mice (*1*) and humans (*14*), the pygmy mutant has normal levels of circulating growth hormone (*15*). However, its usefulness as a model to elucidate the unknown biochemical nature of the African pygmy phenotype and the growth hormone–resistant human dwarf syndromes (*15*) has been limited by the lack of any molecular analysis. Cloning of the pg locus and the eventual identification of the gene product will assist in defining the utility of the pygmy mutant for these studies. In addition, the mutant mouse could be used as a molecularly authentic version of the relevant human dwarf syndrome to develop various therapeutic regimes to alleviate the symptoms of that disease.

REFERENCES AND NOTES

1. M. C. Green, in *Genetic Variants and Strains of the Laboratory Mouse*, M. C. Green, Ed. (Gustav Fischer Verlag, Stuttgart, 1981), pp. 12–278.
2. T. F. Koulewski *et al.*, *Proc. Natl. Acad. Sci. U.S.A.* **86**, 3709 (1989), and references therein.
3. L. Covarrubias *et al.*, *ibid.* **83**, 6020 (1986); L. Covarrubias, Y. Nishida, M. Terao, P. D'Eustachio, B. Mintz, *Mol. Cell. Biol.* **7**, 2243 (1987); T. M. Wilkie and R. D. Palmiter, *ibid.*, p. 1646.
4. R. D. Palmiter and R. L. Brinster, *Annu. Rev. Genet.* **20**, 465 (1986).
5. The incidence of mini-mice in line A was 37 out of 172, and χ^2 analysis gave $0.25 < P < 0.5$; in line B, 38 out of 163 gave $0.5 < P < 0.75$; and matings between hemizygous A and B, 45 out of 187, gave $0.5 < P < 0.75$.
6. A more detailed histological and morphological analysis of the mutant is given by K. Benson and K. Chada (in preparation).
7. M. Low, K. Benson, K. Chada, unpublished data.
8. Preparative gel electrophoresis was performed on 160 μg of Eco R1–digested hemizygous A DNA, and the region containing the 6.0-kb fragment was eluted from the gel and cloned into the lambda ZAP vector (Stratagene). Then, 3×10^5 phage were screened with the transgene, and two positive phage were isolated. The phage were then converted to plasmids, ZAP1 and ZAP2, by "zapping" (Stratagene), and only ZAP1 was further characterized.
9. X. Xiang, K. Benson, K. Chada, unpublished data.
10. J. W. MacArthur, *Am. Nat.* **78**, 142 (1944).
11. N. Copeland *et al.*, unpublished data.
12. A χ^2 analysis gave $0.9 < P < 0.95$ and $0.1 < P < 0.25$ for A and B matings, respectively.
13. K. Benson and K. Chada, unpublished data.
14. V. A. McKusick, *Mendelian Inheritance in Man* (Johns Hopkins Univ. Press, Baltimore, ed. 7, 1986).
15. Y. N. Sinha, G. L. Wolff, S. R. Baxter, O. E. Domon, *Proc. Soc. Exp. Biol. Med.* **162**, 221 (1979).
16. Genomic DNA was isolated from mouse tails [B. Hogan, F. Costantini, E. Lacy, *Manipulating the Mouse Embryo, A Laboratory Manual* (Cold Spring Harbor Laboratory, Cold Spring Harbor, NY, 1986)] and for Southern blot analysis was digested with Eco RI (which cleaves the transgene once), electrophoresed on 0.8% agarose gels, transferred to nitrocellulose, and hybridized with the appropriately labeled probe [T. Maniatis, E. F. Fritsch, J. Sambrook, *Molecular Cloning: A Laboratory Manual* (Cold Spring Harbor Laboratory, Cold Spring Harbor, NY, 1982)]. Hemizygous and homozygous mice were distinguished by quantitative dot blot hybridization with scintillation counting, and the DNA amount was determined by the diaminobenzoic acid fluorimetric assay (B. Hogan *et al.*, above). Control dots containing known amounts of the transgene were used to determine copy number, which was approximately 26 and 21 copies for line A and B, respectively.

17. We thank W. Beamer for the pygmy mice and E. Geissler for the c-*kit*. K.C. is a Basil O'Connor Starter Scholar (Colonel Sanders Memorial Fund). Supported by NIH grant GM38731, New Jersey Commission Cancer Research (687-006), and the Center for Advanced Biotechnology and Medicine.

17 October 1989; accepted 21 December 1989

Atrionatriuretic Peptide Transforms Cardiac Sodium Channels into Calcium-Conducting Channels

LISA ANN SORBERA AND MARTIN MORAD*

The atrionatriuretic peptide (ANP) is released from atrial cells in response to increased extracellular fluid volume and reduces sodium absorption by the kidney, thus reducing the blood volume. In this report, ANP suppressed the calcium and sodium currents in rat and guinea pig ventricular myocytes. The suppression of sodium current was caused by enhanced permeability of the sodium channel to calcium without significant changes in the kinetics or the tetrodotoxin sensitivity of the channel. Thus, ANP may regulate the sodium channel by altering its cationic selectivity site to calcium, thereby repressing the sodium current. The suppression of sodium and calcium channels and the resultant depressed excitability of the atrial cells may help to regulate ANP secretion.

THE SODIUM CHANNEL IS ESSENTIAL for the excitability of nerve, muscle, and heart cells (*1, 2*). The modulation of cardiac Na^+ channels by pharmacological agents has served as the basis for clinical treatment of myocardial arrhythmias (*3*). The physiological regulation of the cardiac Na^+ channel is not well understood, although phosphorylation of the Na^+ channel by an adenosine 3′,5′-monophosphate

(cAMP)–dependent mechanism or through a regulatory G protein may lead to its inactivation (*4, 5*). In this report, we provide evidence for another regulatory mechanism of cardiac Na^+ channels, which is mediated by an alteration of its ionic selectivity by ANP. ANPs are a family of vasoactive peptides that are secreted by atrial cells (*6, 7*), which, in addition to the regulation of Na^+ transport in the kidney, may modulate the Na^+ channels of atrial cells themselves.

Ventricular myocytes were isolated from adult rat or guinea pig hearts (*8*). Myocytes were placed in a chamber coated with fibronectin in order to stabilize them mechanically, making it possible to exchange the bathing solution around individual cells rapidly, with an electronically controlled, multibarreled concentration-clamp system (*9*). The quiescent myocytes were clamped in the whole-cell configuration (*10*) with patch pipettes with tip resistances of 1 to 2 megohms. The cell capacitance ranged between 100 and 300 pF. The composition of extracellular solutions and internal dialysates was dictated by the experimental requirements (*11*), but generally K^+ was omitted from both external and internal solutions and was replaced by either Cs^+ or *N*-methyl glucamine. Intracellular Ca^{2+} was buffered with 14 m*M* EGTA and intracellular H^+ was buffered with 10 to 20 m*M* Hepes, at *p*H 7.2. All experiments were carried out at room temperature. Rat myocytes were usually used, although the results were also confirmed on guinea pig ventricular cells. ANP (rat atrial natriuretic factor, amino acids 1 to 28) was obtained from Peninsula Labs (San Diego, California). The potency varied from lot to lot.

Application of 100 n*M* ANP rapidly suppressed the Na^+ current of a rat ventricular myocyte that had been activated by a depolarizing pulse from −80 to −40 mV (Fig. 1A). The suppressive effect of ANP was often complete within 5 s (n = 62 cells), which was the repeat interval of the clamp pulse in these studies (Fig. 1A). We did not critically investigate the minimal time required for the ANP action, but the effects reversed equally quickly on removal of ANP.

In the presence of 100 n*M* ANP, the Na^+ channel activity was suppressed from 5.5 ± 0.46 to 1.7 ± 0.3 nA (mean ± SEM, n = 35) and at 10 n*M* (n = 22), the amplitude of the Na^+ current (I_{Na}) was reduced from 3.4 ± 0.43 to 2.1 ± 0.3 nA (mean ± SEM, n = 11), whereas at 1 n*M* the channel was not significantly suppressed (n = 4). ANP at 100 n*M* often completely suppressed the Na^+ current at all potentials tested (Fig. 1, B and D). Calcium current (I_{Ca}) was also similarly suppressed by ANP at all membrane potentials tested (Fig. 1, C and D). The kinetics of the ANP effect on I_{Ca} were somewhat slower than those for I_{Na} (20 s versus 2 to 5 s), consistent with the possibility that ANP-induced suppression of I_{Ca} was guanosine 3′,5′-monophosphate (cGMP)–mediated (*12*).

In experiments where I_{Na} was suppressed by only about 75%, the voltage dependence of its activation and its steady-state inactivation were not significantly altered (n = 5). In some cells, however, a 10-mV shift toward more negative potentials was observed.

To differentiate among the likely mechanisms by which ANP may suppress the Na^+ current, we examined the effect of ANP on I_{Na} in the presence or absence of Ca^{2+} in the bathing solutions. In solutions containing 20 μ*M* Ca^{2+}, ANP had either no effect on I_{Na} (n = 7) or suppressed the current by only 5 to 10% (n = 3) whether Mg^{2+} was omitted or included in the bathing solutions. ANP (100 n*M*) had only a minor effect on the Na^+ channel in low Ca^{2+} solutions (Fig. 2). These results suggest that ANP does not directly block the Na^+ channel; rather, the inhibitory action of ANP appears to require calcium.

Given that the Na^+ channel has a finite permeability to Ca^{2+} (*13–15*), one possible mechanism by which ANP could suppress the Na^+ channel is through the enhance-

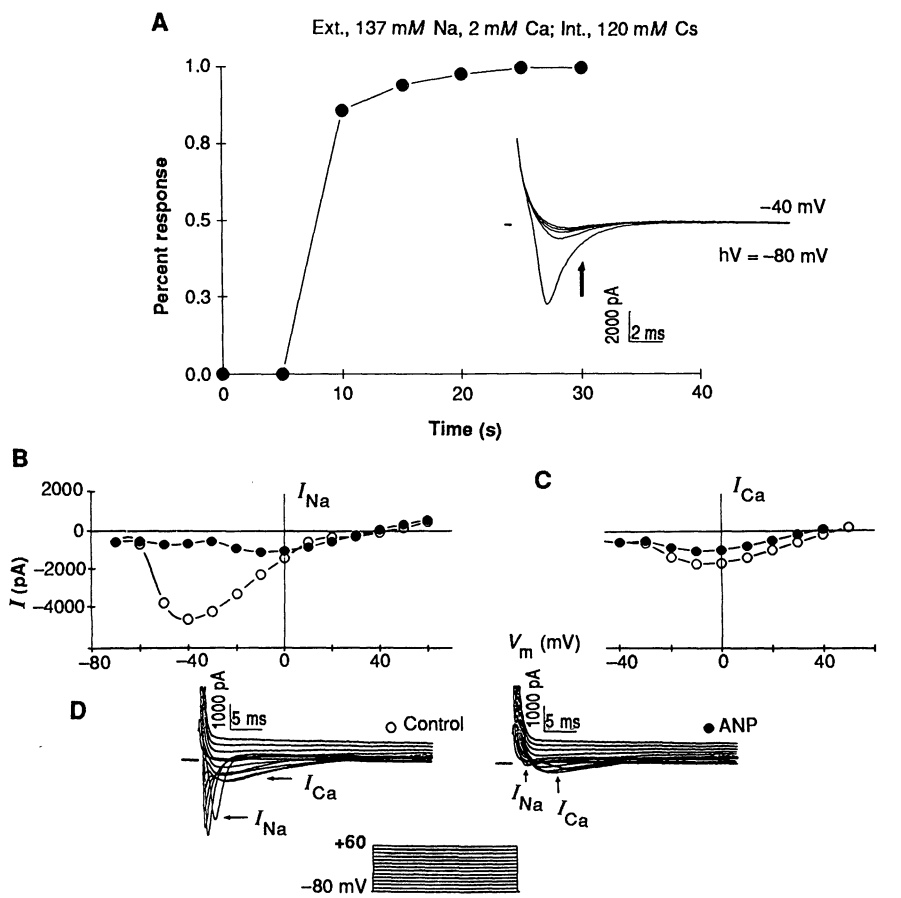

Fig. 1. Effect of ANP on the Na^+ current of rat ventricular myocytes. (**A**) Time course of suppression of the amplitude of the whole-cell sodium current (I_{Na}) by 100 n*M* ANP applied 1 to 2 s after the control measurement at 5 s. Na^+ current was activated by 30-ms depolarizing pulses to −40 mV from a holding potential (hV) of −80 mV (inset). Clamp pulses were applied at 5-s intervals. Arrow indicates direction of ANP-induced response. (**B**) The voltage dependence of I_{Na} in control solution (○) and in the presence of ANP (●). (**C**) The voltage dependence of I_{Ca}, showing the suppressive effect of ANP (●) as compared to control (○). (**D**) Tracings of membrane currents activated from −80 to +60 mV (at bottom) in control (left) and ANP-containing (100 n*M*) (right) solutions. In control solutions both the faster Na^+ and the slower Ca^{2+} current are easily detectable. In the presence of ANP, the faster inward current is completely suppressed while the slower current, although somewhat suppressed, is easily distinguishable. Temperature, 24°C. Currents are measured from the actual zero reference. Holding current, 200 pA at −80 mV. The recorded currents are not corrected for capacitance or leak currents. External solution: 137 m*M* NaCl; 0 KCl; 1.0 m*M* $MgCl_2$; 2 m*M* $CaCl_2$; 10 m*M* Hepes; and 10 m*M* glucose, *p*H 7.4. Internal solution: 120 m*M* CsCl; 5 m*M* MgATP; 20 m*M* Hepes; 14 m*M* EGTA; and 1 μ*M* cAMP, *p*H 7.2.

Department of Physiology, University of Pennsylvania, Philadelphia, PA 19104–6085 and Mount Desert Island Biological Laboratory, Salsbury Cove, ME 04672.

*To whom correspondence should be addressed.

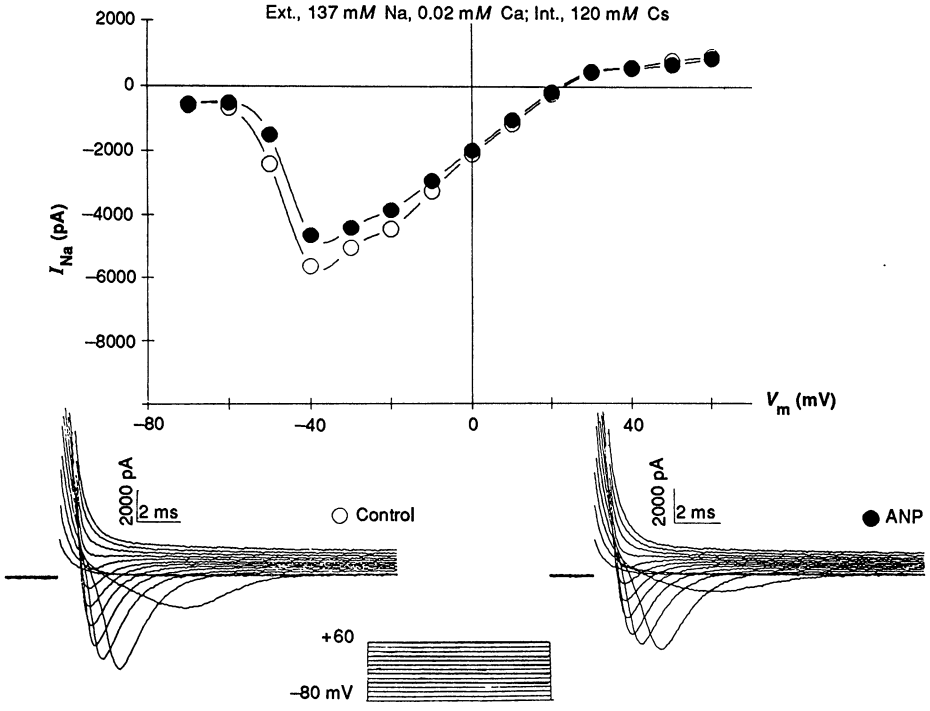

Fig. 2. The effect of ANP in the absence of extracellular Ca^{2+}. Voltage dependence of I_{Na} in the presence (○) and absence (●) of ANP. Although there is some small alteration of I_{Na} by ANP, the Na^+ current remained mostly unaffected (compare with Fig. 1, where $[Ca^{2+}]_o$ was 2 m*M*). Clamp pulses were applied at 5-s intervals, and the duration of the depolarization pulse was 35 ms. Bottom, insets are superimposed tracings of membrane currents activated from −80 to +60 mV (at bottom) in control solution and solution containing 100 n*M* ANP where extracellular Ca^{2+} was 20 μ*M*. The extracellular Ca^{2+} concentration is most likely higher than the indicated value, as 20 μ*M* Ca^{2+} was added to nominally zero Ca^+ solutions. External solution: 137 m*M* NaCl; 0 KCl; 10 m*M* $MgCl_2$; 0.02 m*M* $CaCl_2$; 10 m*M* Hepes; and 10 m*M* glucose, *p*H 7.4. Internal solution: 120 m*M* CsCl; 5 m*M* MgATP; 20 m*M* Hepes; 14 m*M* EGTA; and 10 μ*M* cAMP, *p*H 7.2.

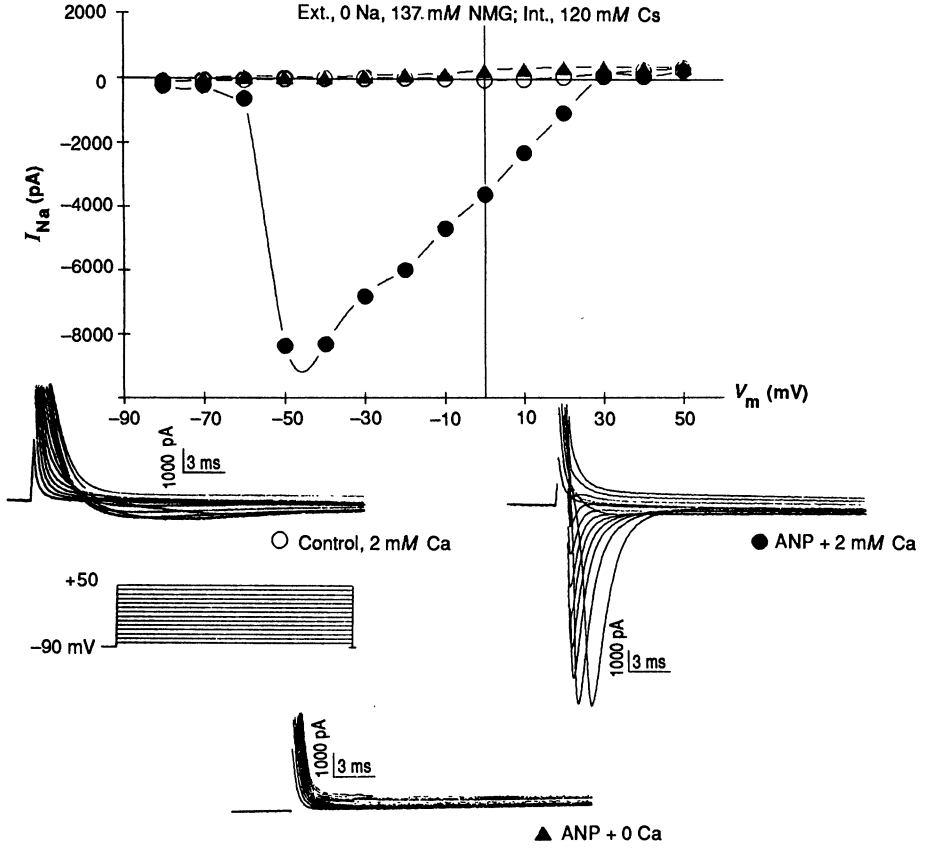

ment of Ca^{2+} permeability of the Na^+ channel. To test for such a possibility, we carried out experiments in which the extracellular Na^+ was completely replaced by Cs^+ or *N*-methyl glucamine. Sodium was omitted from external and internal solutions before the addition of ANP (Fig. 3). The records obtained in Na^+-free (but Ca^{2+}-containing) solutions showed only the slowly activating and inactivating Ca^{2+} current (Fig. 3). Addition of 100 n*M* ANP activated a large rapidly activating and inactivating current from 0.21 ± 0.04 to 3.8 ± 0.5 nA (mean ± SEM, $n = 47$) with kinetics and voltage dependence similar to those generally associated with the Na^+ channel (Fig. 3). This inward current was completely suppressed in the absence of extracellular Ca^{2+} (Fig. 3), suggesting that Ca^{2+} was the charge carrier.

We also compared the relative sensitivity of ANP-activated Ca^{2+} current through the Na^+ channel to blockers of Ca^{2+} (10 μ*M* nifedipine or 5 m*M* Ni^{2+}) or Na^+ channels [10 μ*M* tetrodotoxin (TTX)]. Depolarizing the cell to 0 mV in the Na^+-free control solution activated only the Ca^{2+} current (Fig. 4A, control trace). Addition of ANP induced a rapidly activating and inactivating inward current (ANP trace), which was followed by the slower I_{Ca} through the Ca^{2+} channel. Exposure of the cell to 5 m*M* Ni^{2+} in the presence of ANP suppressed I_{Ca} through the Ca^{2+} channel (Fig. 4B), but had no effect on the rapidly activating inward current (trace ANP + Ni^{2+}). Since Ca^{2+} was the only permeant cation and the Ca^{2+} channels were already blocked by Ni^{2+}, it was concluded that the rapidly

Fig. 3. ANP activates a Ca^{2+} current through the Na^+ channel in zero Na^+ solutions. The voltage dependence of the rapid inward current is plotted under three conditions. In the absence of Na^+ and with 2 m*M* Ca^{2+} the current-voltage (*I-V*) relation of I_{Na} is flat (○), but in the presence of ANP (100 n*M*) we measured a large inward current (which was difficult to control) with peak around −40 mV and a reversal of potential positive to +30 mV (●). ▲, The *I-V* relation for the current in the absence of Ca^{2+} but in the presence of ANP. Note that the inward current through the Na^+ channel is completely suppressed in the absence of Ca^{2+}. Clamp pulses were applied at 5-s intervals with a duration of 35 ms. Temperature, 24°C. Tracings are superimposed membrane currents activated from −90 to +50 mV (inset) in the indicated solutions. In the absence of extracellular Na^+ but with 2 m*M* Ca^{2+} (○), only a slowly activating inward Ca^{2+} current is measured. Addition of ANP to such a solution activates a rapidly inactivating current through the Na^+ channel in excess of 8 nA (●). The current is completely suppressed when Ca^{2+} is absent (▲). External solution: 0 Na; 137 m*M* *N*-methyl glucamine (NMG); 0 KCl; 1.0 m*M* $MgCl_2$; 10 m*M* Hepes; and 10 m*M* glucose, *p*H 7.4; Ca^{2+} is specified in figure. Internal solution: 120 m*M* CsCl; 5 m*M* MgATP; 20 m*M* Hepes; 14 m*M* EGTA; and 10 μ*M* cAMP, *p*H 7.2.

activating and inactivating current was also carried by Ca^{2+}, but through the Na^+ channels. This Ca^{2+}-carrying channel was suppressed by TTX (10 μM).

In experiments where extracellular sodium ion concentrations were reduced to 10 mM, the ANP-induced enhancement of the Na^+ current was also blocked by TTX (Fig. 4, C and D). Under such conditions, depolarizing pulses from −90 to −40 mV activated a small Na^+ current (Fig. 4C, control trace), which reversed at 0 mV the electrochemical potential for Na^+ (not shown). Addition of ANP activated a rapidly inactivating current, which was blocked completely by addition of 10 μM TTX (Fig. 4D). The reversal potential of the ANP-enhanced current, however, shifted from 0 to about +40 mV, far above the electrochemical equilibrium potential for Na^+ (E_{Na}) (n = 15). The shift in the reversal potential in conjunction with the blocking of the channel by TTX implicated the Na^+ channel as the channel conducting the Ca^{2+} current. In such experiments, the kinetics of Na^+ channel current once again remained unaltered.

Thus, ANP induces a molecular transformation in the Na^+ channel that renders the channel highly permeable to Ca^{2+}. The transformation of the channel selectivity did not require the presence of Na^+ extracellularly or intracellularly. The suppressive effect of ANP on the Na^+ current in normal extracellular Na^+, and the enhancement of the channel current by ANP when extracellular Na^+ is below 10 mM, are consistent with the altered Ca^{2+} selectivity of the Na^+ channel. The molecular transformation appears to occur rapidly and was reversible equally rapidly upon removal of ANP, suggesting an extracellular site of activation. It is not yet clear whether the ANP-induced transformation in the selectivity of the Na^+ channel occurs as a result of a direct interaction of ANP with the channel protein or is mediated by activation of a regulatory G protein. In pertussis toxin–treated cells (500 ng/ml, 5 hours incubation at 24°C) or in myocytes where guanosine 5′-O-(2-thiodiphosphate) (GDPβS) or guanosine 5′-O-(3-thiotriphosphate) (GTPγS) was included in the patch pipette to suppress or enhance the G protein–regulated reactions, we did not see a change in the ANP-induced effects. Further, the mechanism appeared to be independent of the phosphorylation state of the Na^+ channel, since including 10 μM cAMP in the internal solution (*4, 5*) did not alter the ANP-induced response. Possible involvement of Cl^- in activation of this current was also ruled out since complete substitution of Cl^- with aspartate did not alter the magnitude of the current.

The simplest explanation of our results is that ANP enhances the Ca^{2+} selectivity of the Na^+ channel. Permeation through the Na^+ channel may occur somewhat similarly to that described for the Ca^{2+} channel (*16–19*). That is, both Na^+ and Ca^{2+} may compete for a permeation site, the selectivity of which would be determined by the conformational state of the channel induced either by ionic or hormonal interventions (Figs. 1 to 3). Thus, alteration in the ionic selectivity of a channel by a hormone may serve as a rapid regulatory mechanism for the conductance of the channel. The combined suppressive effects of ANP on Na^+ and Ca^{2+} channels may render the secretory atrial tissues inexcitable and noncontracting.

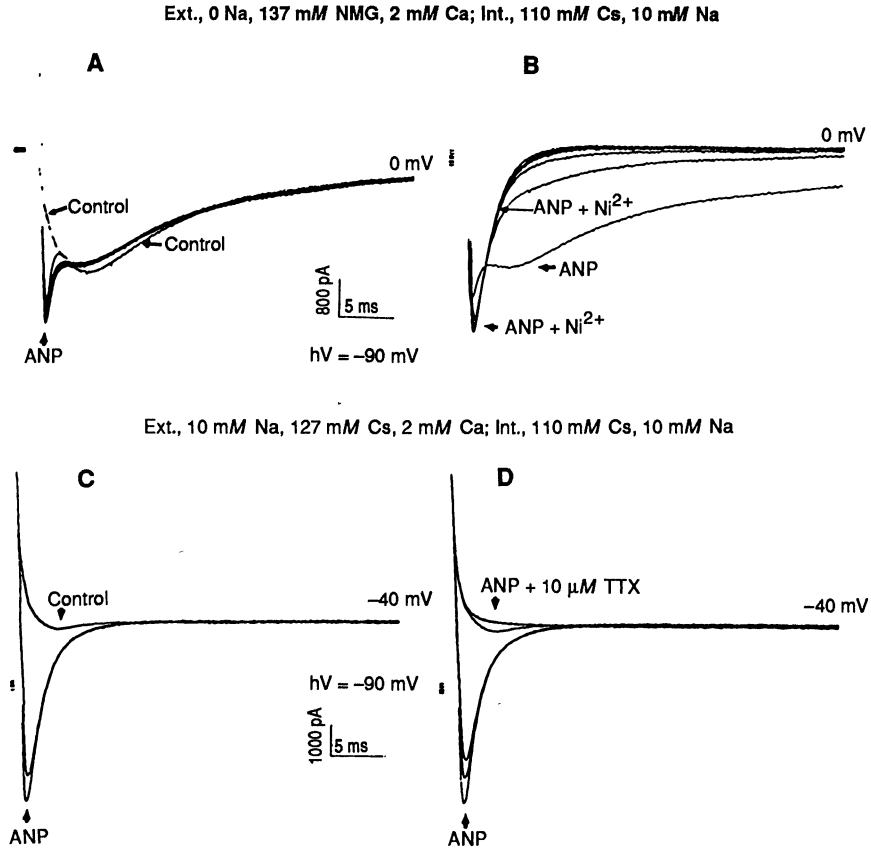

Fig. 4. Comparison of kinetics of ANP-induced inward current with those of Ca^{2+} and Na^+ channels. (**A**) Inward currents activated at 0 mV in the absence of Na^+ and with 2 mM Ca^{2+}, before (control trace) and after addition of ANP (ANP trace). Note that a rapidly inactivating current is activated by ANP, which is then followed by a somewhat suppressed and slower Ca^{2+} current. (**B**) The same cell is then exposed to 5 mM Ni^{2+}, which blocks the Ca^{2+} channel leaving the rapidly inactivating Na^+ channel current unaltered. (**C**) The TTX sensitivity of ANP-induced transformation in Na^+ channel permeability is tested in a solution containing 10 mM Na^+ and 2 mM Ca^{2+}. In the absence of ANP, the Na^+ channel current at −40 mV is small. Application of ANP enhances the current markedly (C), which is then completely blocked by TTX (**D**). hV, holding potential. (A and B) External solution: 0 Na; 137 mM *N*-methyl glucamine (NMG); 0 KCl; 1.0 mM $MgCl_2$; 2 mM $CaCl_2$; 10 mM Hepes; and 10 mM glucose, *p*H 7.4. Internal solution: 110 mM CsCl; 10 mM NaCl; 5 mM MgATP; 14 mM EGTA; 20 mM Hepes; and 1 μM cAMP, *p*H 7.2. (C and D) External solution: 10 mM NaCl; 127 mM $CsCl_2$; 0 KCl; 1.0 mM $MgCl_2$; 2 mM $CaCl_2$; 10 mM Hepes; and 10 mM glucose, *p*H 7.4. Internal solution: 110 mM CsCl; 10 mM NaCl; 5 mM MgATP; 20 mM Hepes; 14 mM EGTA; and 1 μM cAMP, *p*H 7.2.

REFERENCES AND NOTES

1. A. L. Hodgkin and A. F. Huxley, *J. Physiol. (London)* **117**, 500 (1952).
2. B. Hille, *Ionic Channels of Excitable Membranes* (Sinauer, Sunderland, MA, 1984).
3. E. M. Vaughan Williams, *J. Clin. Pharmacol.* **24**, 129 (1984).
4. W. A. Catterall, *Science* **242**, 50 (1988).
5. B. Schubert, A. M. J. VanDongen, G. E. Kirsch, A. M. Brown, *Science* **245**, 516 (1989).
6. A. J. Debold, H. B. Borenstein, A. T. Veress, H. Sonnenberg, *Life Sci.* **28**, 89 (1981).
7. G. E. Ballermann and B. M. Brenner, *Circ. Res.* **58**, 619 (1986).
8. R. Mitra and M. Morad, *Am. J. Physiol.* **249**, H1056 (1985).
9. A. Konnerth, H. D. Lux, M. Morad, *J. Physiol. (London)* **386**, 603 (1987); C.-M. Tang, M. Dichter, M. Morad, *Science* **243**, 1474 (1989).
10. O. P. Hamill, A. Marty, E. Neher, B. Sakmann, F. J. Sigworth, *Pfluegers Arch.* **395**, 6 (1981).
11. Internal solution contained 120 mM CsCl, 5 mM magnesium adenosine triphosphate (MgATP), 0.01–0.001 mM cAMP, 14 mM EGTA, and 10 to 20 mM Hepes buffer, *p*H 7.2, with CsOH. Standard external solution contained 137 mM NaCl, 2 mM $CaCl_2$, 1 mM $MgCl_2$, 10 mM glucose, and 10 mM

Hepes buffer titrated to pH 7.4 by addition of NaOH.
12. M.-P. Gisbert and R. Fishmeister, *Circ. Res.* **62**, 660 (1988).
13. H. Meves and W. Vogel, *J. Physiol. (London)* **235**, 225 (1973).
14. A. M. Woodhull, *J. Gen. Physiol.* **61**, 687 (1973).
15. B. Nilius, *J. Physiol. (London)* **399**, 537 (1988).
16. P. Hess and R. W. Tsien, *Nature* **309**, 453 (1984).
17. W. Almers, E. W. McCleskey, P. T. Palade, *J. Physiol. (London)* **353**, 565 (1984).
18. H. D. Lux, E. Carbone, H. Zucker, in *The Calcium Channel: Structure, Function and Implications*, M. Morad *et al.*, Eds. (Springer-Verlag, Heidelberg, 1988), pp. 128–137.
19. P. G. Kostyuk, S. L. Mironov, Y. M. Shuba, *J. Membr. Biol.* **76**, 83 (1983).
20. Supported by NIH grant HL16152.

4 October 1989; accepted 5 December 1989

A Family of Three Mouse Potassium Channel Genes with Intronless Coding Regions

K. GEORGE CHANDY, CALVIN B. WILLIAMS, ROBERT H. SPENCER, BARBARA A. AGUILAR, SANJIV GHANSHANI, BRUCE L. TEMPEL, GEORGE A. GUTMAN

To understand the molecular mechanisms responsible for generating physiologically diverse potassium channels in mammalian cells, mouse genomic clones have been isolated with a potassium channel complementary DNA, MBK1, that is homologous to the *Drosophila* potassium channel gene, *Shaker*. A family of three closely related potassium channel genes (*MK1*, *MK2*, and *MK3*) that are encoded at distinct genomic loci has been isolated. Sequence analysis reveals that the coding region of each of these three genes exists as a single uninterrupted exon in the mouse genome. This organization precludes the generation of multiple forms of the protein by alternative RNA splicing, a mechanism known to characterize the *Drosophila* potassium channel genes *Shaker* and *Shab*. Thus, mammals may use a different strategy for generating diverse K^+ channels by encoding related genes at multiple distinct genomic loci, each of which produces only a single protein.

SEVERAL CLASSES OF K^+ CHANNELS are involved in maintaining membrane potential and regulating cell volume in diverse cell types, as well as modulating electrical excitability in the nervous system (*1*). The molecular mechanisms generating K^+ channel diversity are best understood in the *Shaker* locus from *Drosophila*, which contains 21 exons spanning 130 kb and generates four different K^+ channel proteins through alternative splicing of a single primary transcript (*2*). Expression of these cDNAs in *Xenopus* oocytes gives rise to voltage-dependent K^+ currents with distinct physiological properties (*3*). The related *Drosophila* K^+ channel gene *Shab* also exhibits alternative splicing of a primary transcript, giving rise to two distinct proteins (*4*). To determine if similar mechanisms are responsible for K^+ channel diversity in mammals, we have isolated and characterized eight mouse genomic clones that contain three related K^+ channel genes (*5–7*), all of which hybridize with the cDNA MBK1 (mouse brain K^+ channel 1) (*8*).

Southern (DNA) transfers (*9*) of Hind III–digested liver DNA from BALB/c mice were hybridized with a 1695-bp probe derived from the MBK1 cDNA that contained the entire 1485-bp coding region (*8*). Three Hind III fragments (8.6 kb, 3.4 kb, and 2.0 kb) hybridized strongly with this probe (Fig. 1). These bands may represent multiple exons, as in the *Shaker* locus (*2*), or each band could represent a unique K^+ channel gene. Shorter probes representing the 5′ and the 3′ portions of the MBK1 coding region (0.5 and 1.1 kb, respectively) yielded a hybridization pattern identical to that obtained with the full-length 1.6-kb probe, suggesting that each of the multiple bands may contain a sequence corresponding to the full-length MBK1 coding region.

To further study the genomic organization of these putative K^+ channel genes, we screened a mouse genomic library (*5, 6*) with the full-length MBK1 cDNA probe (*8*). Of the eight genomic clones characterized thus far (*5, 6*), four, containing hybridizing Hind III fragments identical in size to those in Fig. 1, are described here: KC250, which contains a 2.0-kb hybridizing fragment; overlapping clones KC238 and KC255 (KC238/255), which contain a 3.4-kb hybridizing fragment; and identical clones KC236 and KC237, which contain an 8.6-kb hybridizing fragment within a 12-kb insert.

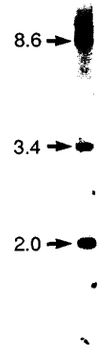

Fig. 1. Southern blot analysis of genomic DNA from BALB/c mice. Liver DNA (10 μg) from BALB/c mice was digested with Hind III, separated on a 0.9% agarose gels, and transferred to nitrocellulose papers by standard procedures (*9, 22*). Southern blots were hybridized with ^{32}P-labeled MBK1 cDNA probes. We used the 0.5-kb Sma I fragment and the 1.1-kb Sma I–Hind III fragments of the MBK1 cDNA (*8*), labeled to a specific activity of 1×10^9 cpm/μg with the random-primer method of Feinberg *et al.* (*23*). Hybridization was performed at 55°C in hybridization buffer for 16 to 18 hours. Hybridization buffer is 5× SSC (*5*), 10× Denhardt's solution [0.2% bovine serum albumin, 0.2% Ficoll and 0.2% polyvinyl pyrrolidone], and 0.1% SDS. The blot was washed at 55°C at a final stringency of 0.2× SSC and 0.1% SDS for 60 min. Exposure time for this autoradiogram was 10 days with an intensifying screen.

We determined the order of restriction fragments of these genomic clones (Fig. 2) by partial digests, by sequencing (*10*), and by aligning the genomic sequence with that of their homologous cDNA sequences. The restriction map of clone KC250 is identical to that of the MBK1 cDNA (*8*) and is similar to the map of the RCK1 (*11*) (the rat cortical K^+ channel 1, a homolog of MBK1) cDNA, in the coding region as well as in the nearby noncoding regions (NCR). The restriction map of the KC238/255 insert is very similar to the map of the RBK2 (rat brain K^+ channel 2) cDNA (*12*). This suggests that KC250 and KC238/255 encode *MK1* and *MK2*, respectively; KC237 appears to encode a related K^+ channel gene.

Partial nucleotide sequences (*10*) of clones KC250 (2222 bp), KC238/255 (3383 bp), and KC237 (2000 bp) were determined. The KC250 sequence is virtually identical to the published MBK1 sequence (*8*) throughout its length (there are additional G's at positions 162 and 442 in the 5′ untranslated region), and is 97.3% identical to RCK1 within the putative coding region (*11*). The entire coding region for this gene, *MK1*, is contained in a single uninterrupted exon of 1485 bp. The 5′ and 3′ NCRs of *MK1* are 91.4% similar to RCK1 (*11*), indicating that the NCRs of *MK1/RCK1* are fairly well conserved. Comparison of KC238/255 with the coding region of RBK2 cDNA reveals 97% sequence identity and shows that the entire coding region of this second gene (*MK2*) is also contained in a single exon of

K. G. Chandy, R. H. Spencer, B. A. Aguilar, S. Ghanshani, Division of Rheumatology and Clinical Immunology, Department of Medicine, University of California, Irvine, CA 92717.
C. B. Williams and G. A. Gutman, Department of Microbiology and Molecular Genetics, University of California, Irvine, CA 92717.
B. L. Tempel, Geriatric Research, Education and Clinical Center, Seattle Veterans Hospital Medical Center, and Departments of Medicine and Pharmacology, University of Washington, Seattle, WA 98108.